(†ESI) Electronic Supplementary Information for

Quasi-2D $Bi_{0.775}Ln_{0.225}O_{1.5}$ (Ln = La, Pr, Nd, Sm, Eu): Reversible iodine intercalation and their evaluation as the anode in the lithium-ion battery system

Priyanka Yadav,[1] Shivangi Rao,[1] O.V. Sreejith,[2] Ramaswamy Murugan[2] and Rajamani Nagarajan[1]*

[1]Materials Chemistry Group, Department of Chemistry

University of Delhi, Delhi-110007 INDIA

[2]High Energy Density Batteries Research Laboratory, Department of Physics, Pondicherry University, Puducherry 605 014, INDIA

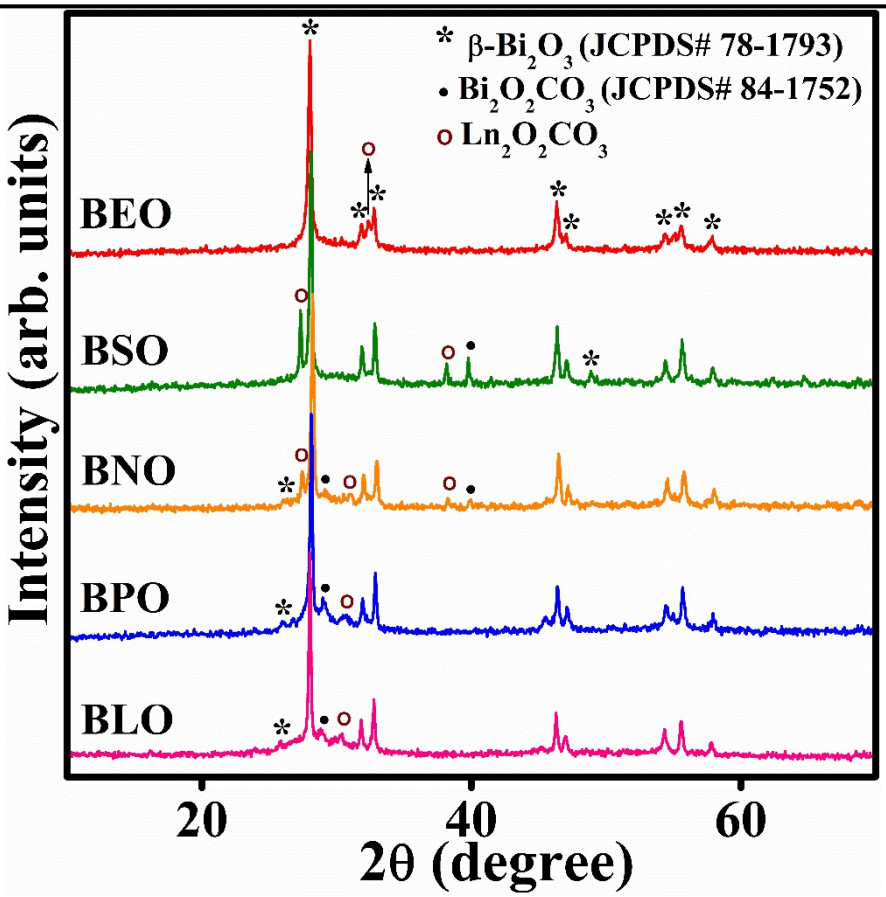

Fig. S1 PXRD patterns of combusted ashes of Bi_2O_3-Ln_2O_3-citric acid complexes. $La_2O_2CO_3$ (JCPDS# 84-1963), $Pr_2O_2CO_3$ (JCPDS# 37-0805), $Nd_2O_2CO_3$ (JCPDS# 37-0806), $Sm_2O_2CO_3$ (JCPDS # 37-0807), and $Eu_2O_2CO_3$ (JCPDS # 25-0334).

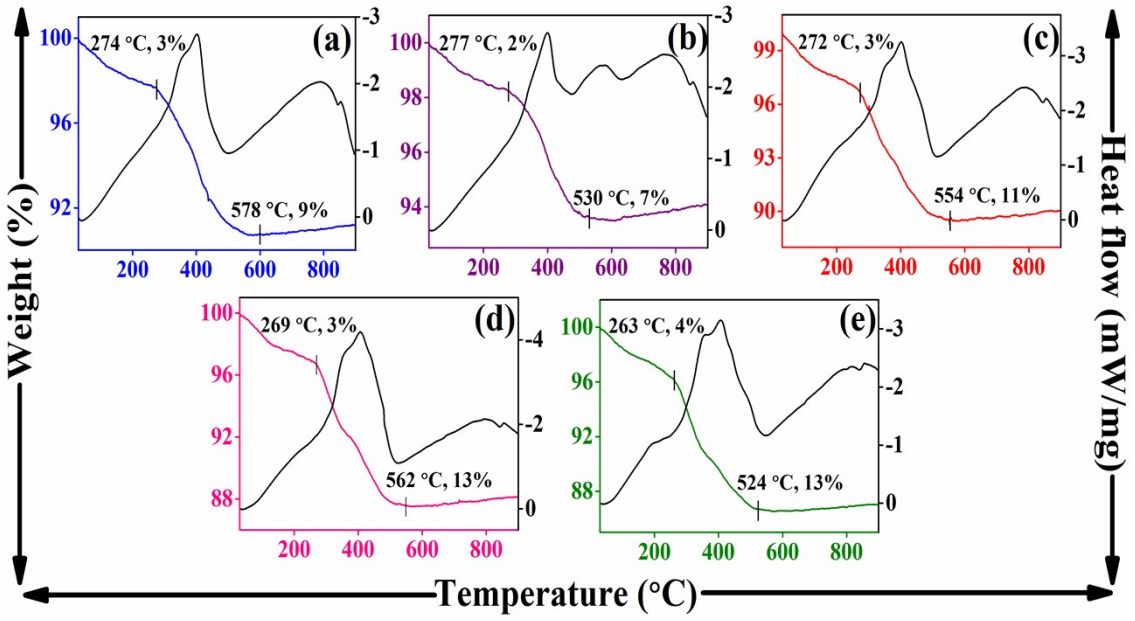

Fig. S2 Simultaneous TG/DSC traces of combusted precursors of bismuth-rare earth metal-citric acid where the rare earth metals are La (a), Pr (b), Nd (c), Sm (d), and Eu (e).

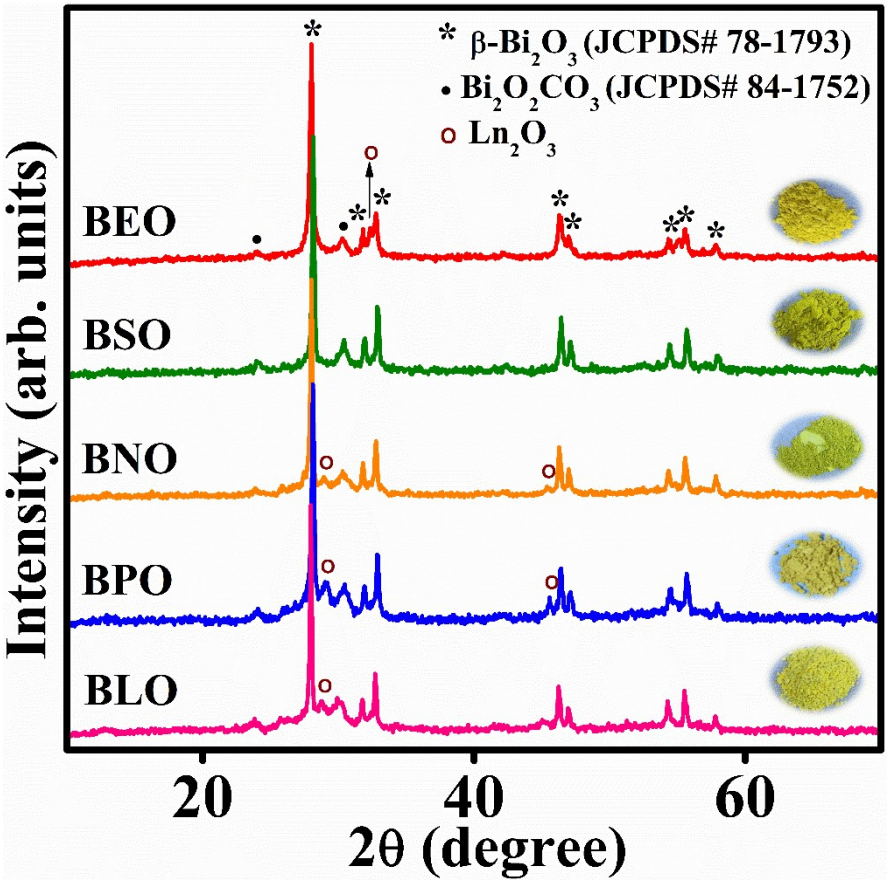

Fig. S3 PXRD patterns of $Bi_{0.775}Ln_{0.225}O_{1.5}$ samples' ashes calcined at 270 °C. La_2O_3 (JCPDS# 83-1355), Pr_2O_3 (JCPDS# 78-0309), Nd_2O_3 (JCPDS# 83-1353), Sm_2O_3 (JCPDS# 19-1114) and Eu_2O_3 (JCPDS# 19-0463).

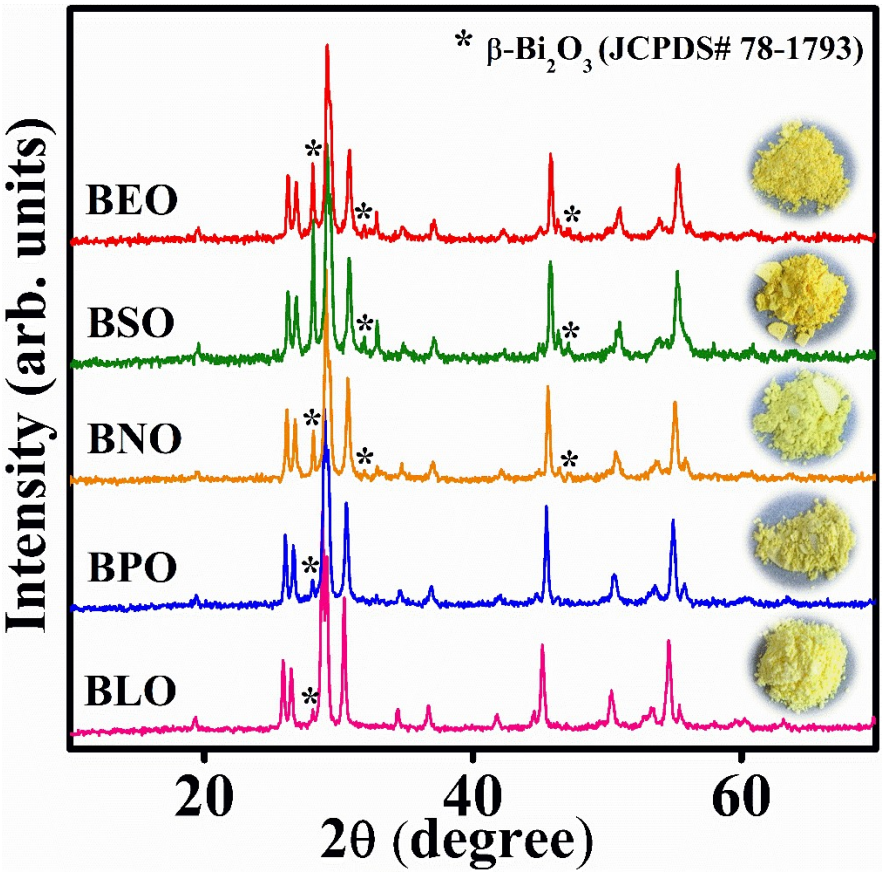

Fig. S4 PXRD patterns of $Bi_{0.775}Ln_{0.225}O_{1.5}$ samples' ashes calcined at 550 °C.

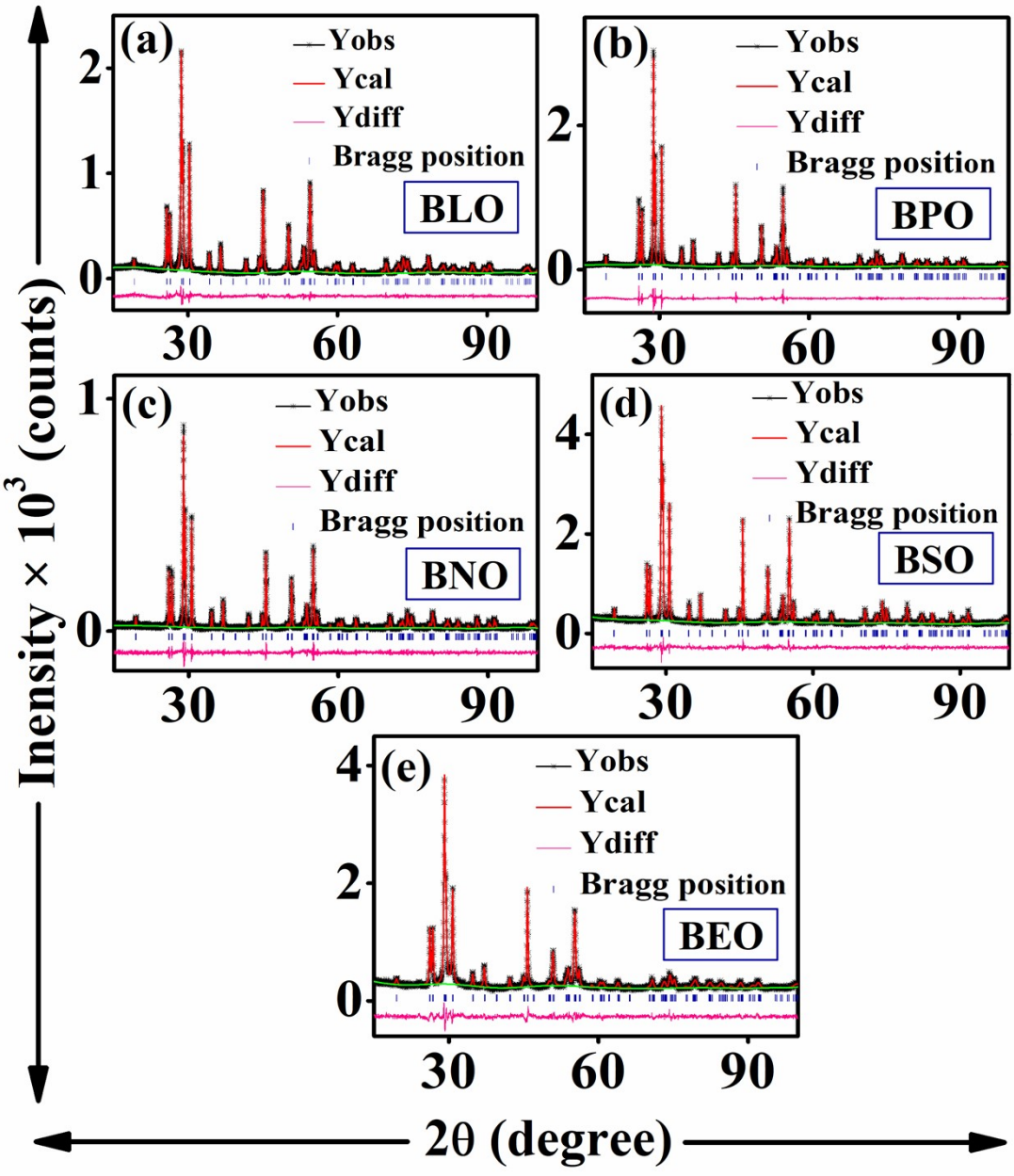

Fig. S5 Lattice refinement of the PXRD patterns of $Bi_{0.775}Ln_{0.225}O_{1.5}$ by the Le Bail method.

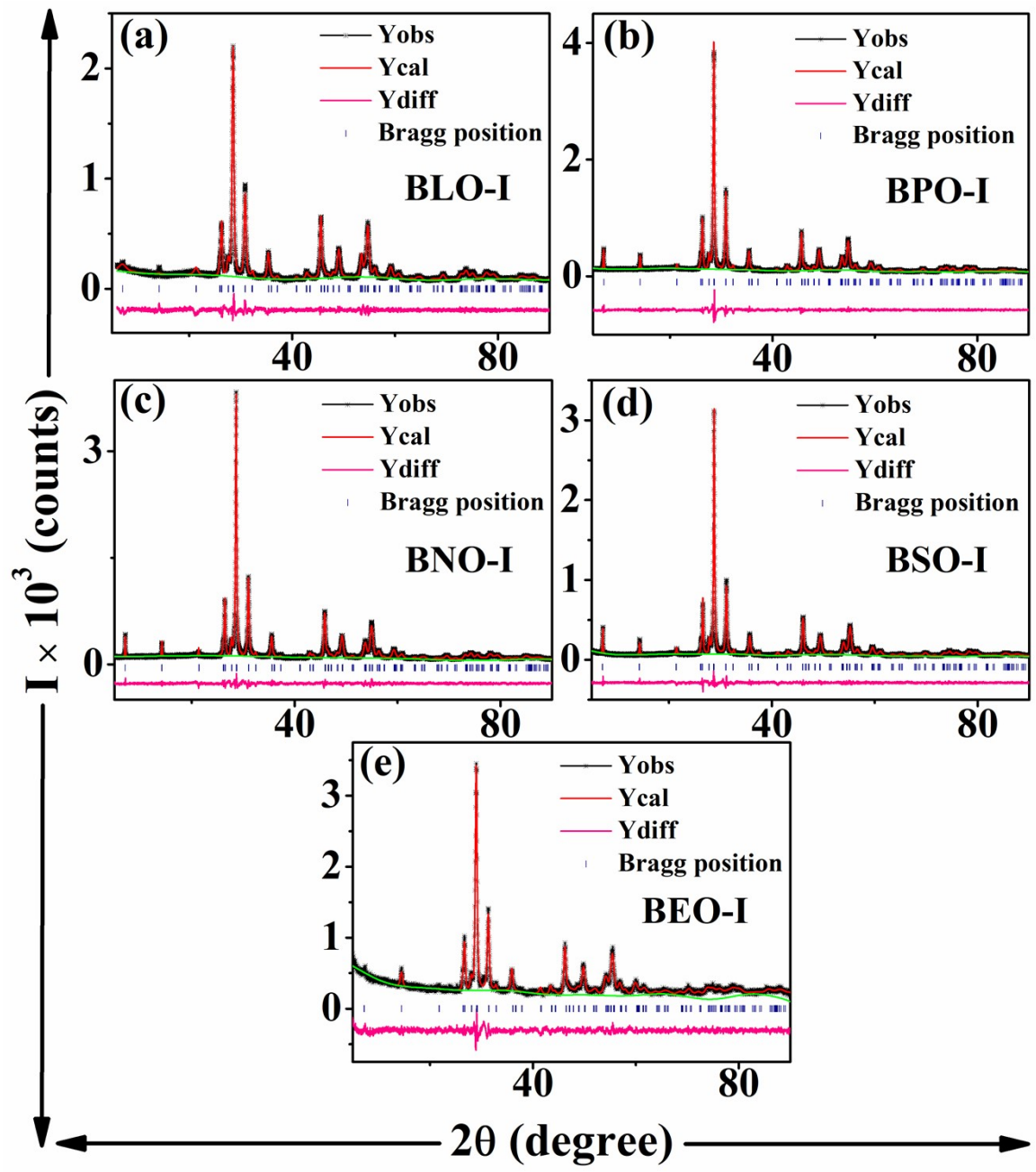

Fig. S6 Lattice refinement of the PXRD patterns of iodine intercalated $Bi_{0.775}Ln_{0.225}O_{1.5}$ by the Le Bail method.

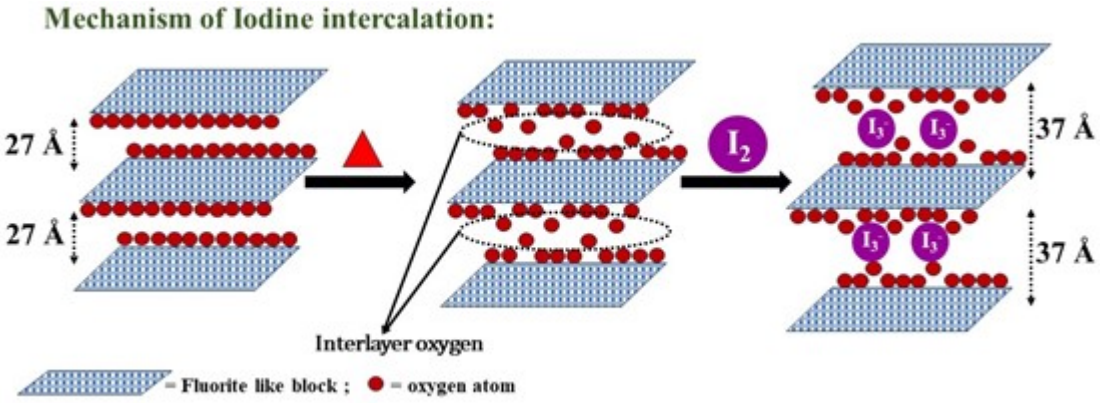

Fig. S7 Schematic representation of steps involved in the intercalation of iodine species in $Bi_{0.775}Ln_{0.225}O_{1.5}$.

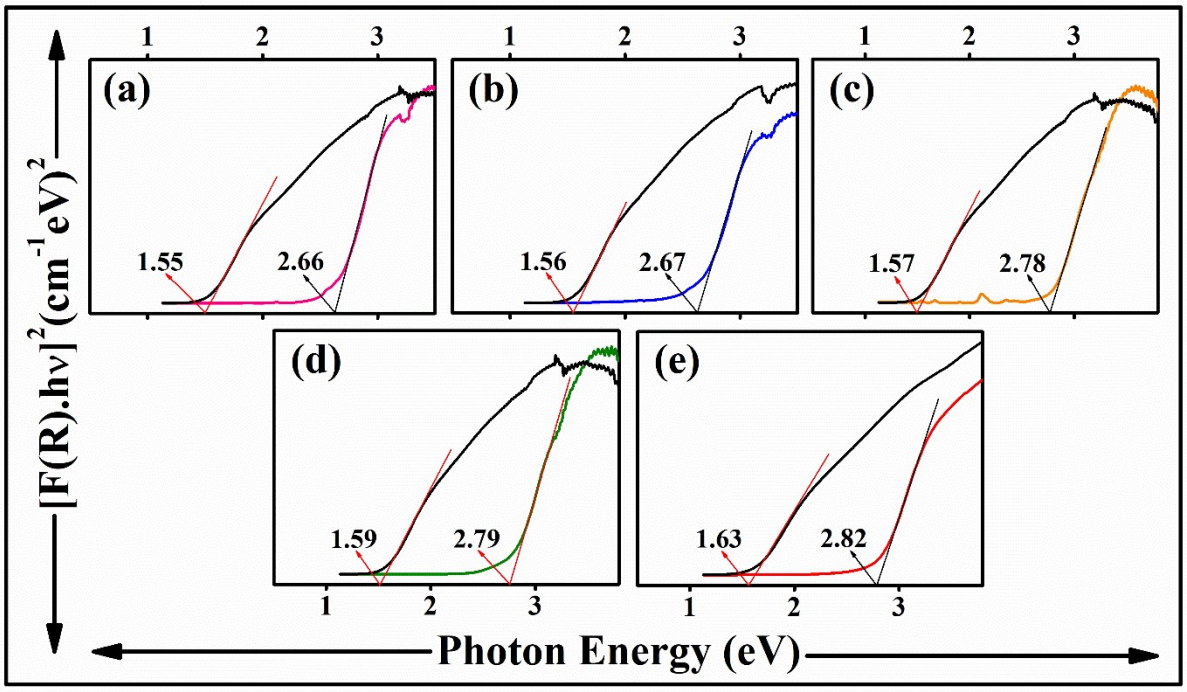

Fig. S8(a)-(e) Bandgap estimation using Tauc plots of BLO, BPO, BNO, BSO, BEO, BLO-I, BPO-I, BNO-I, BSO-I, and BEO-I samples.

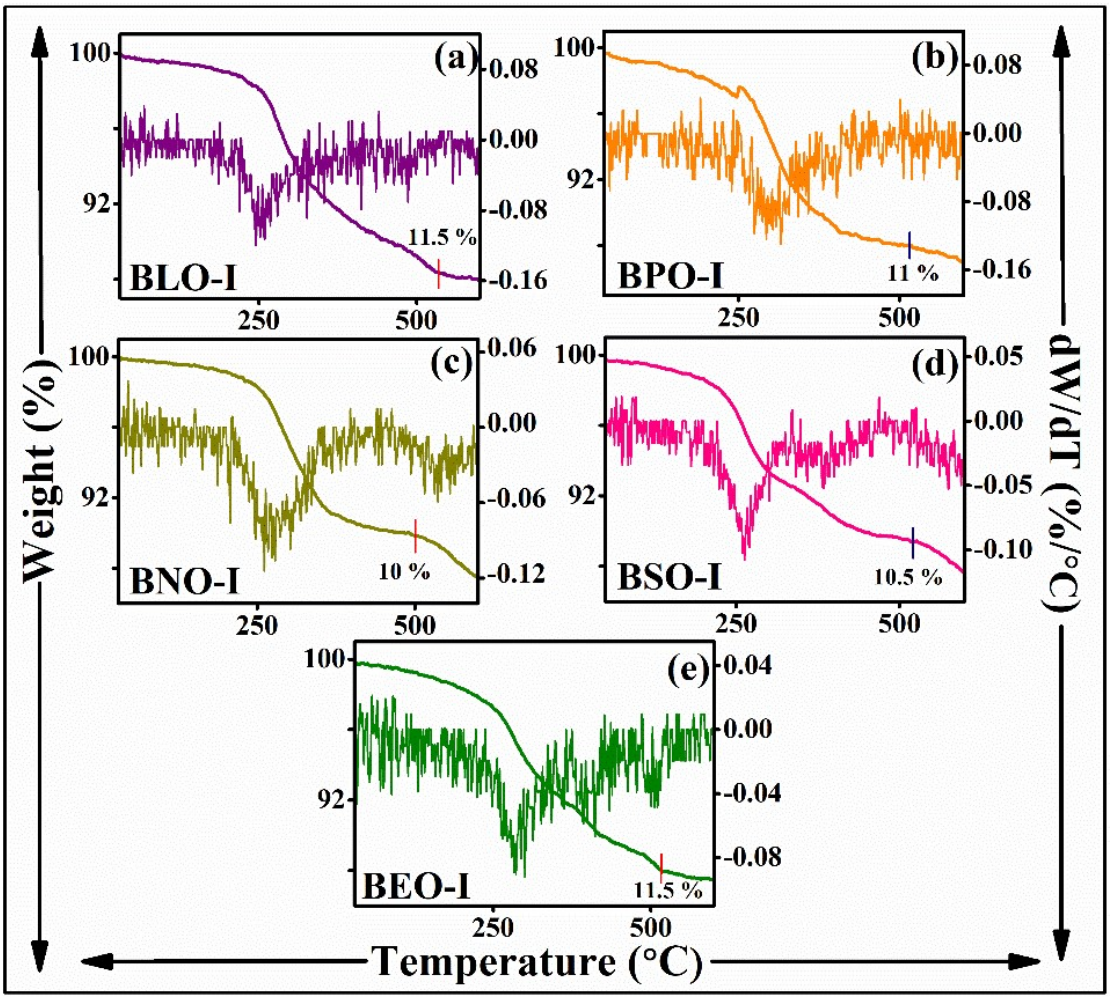

Fig. S9 Thermogravimetric and derivative thermogravimetric traces of BLO-I, BPO-I, BNO-I, BSO-I, and BEO-I samples.

Sample	Combusted ashes	Calcined ashes	Product after iodine intercalation	Product after iodine de-intercalation
BLO				
BPO				
BNO	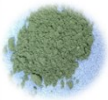			
BSO	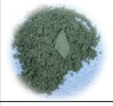			
BEO*				

* calcined at 600 °C

Fig. S10 Digital images of the combusted ashes, calcined products, products after iodine intercalation, and products after thermal iodine deintercalation of $Bi_{0.775}Ln_{0.225}O_{1.5}$ samples.

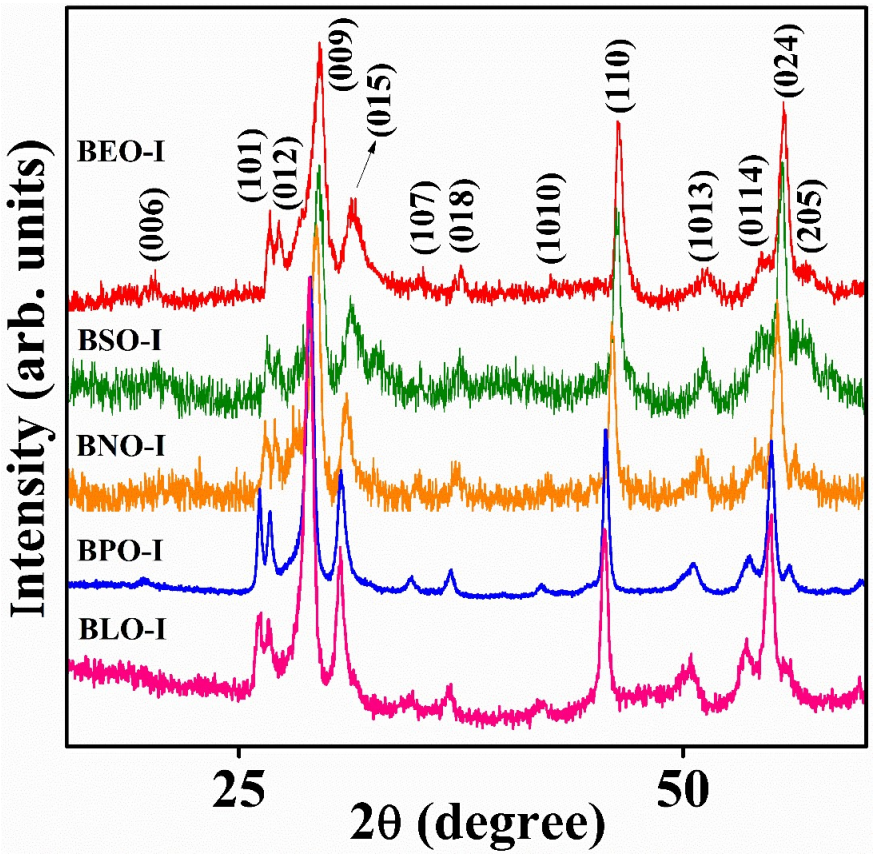

Fig. S11 PXRD patterns of iodine intercalated $Bi_{0.775}Ln_{0.225}O_{1.5}$ samples after calcination in air at 600 ºC for 6 h.

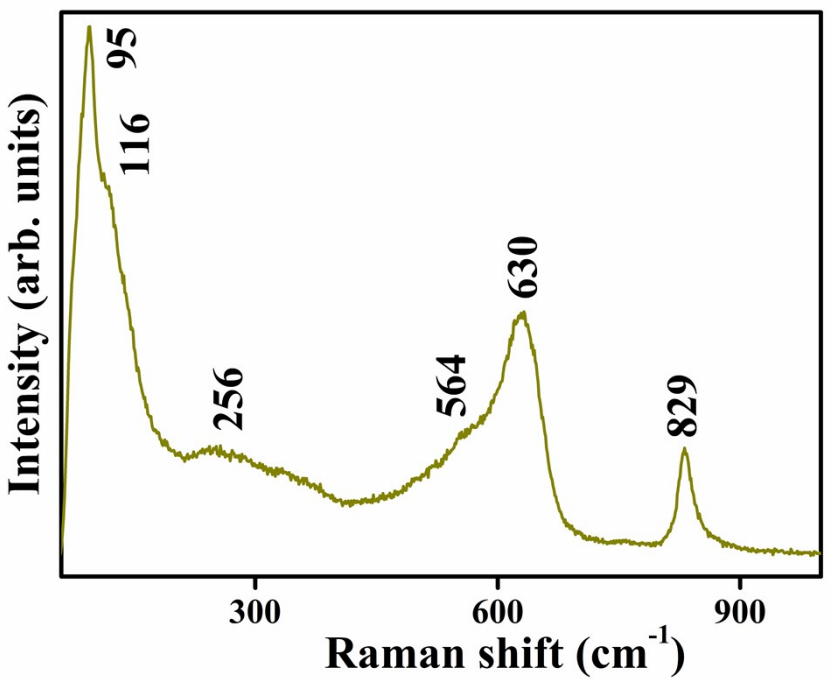

Fig. S12 Raman spectrum of iodine deintercalated $Bi_{0.775}Pr_{0.225}O_{1.5}$ sample.

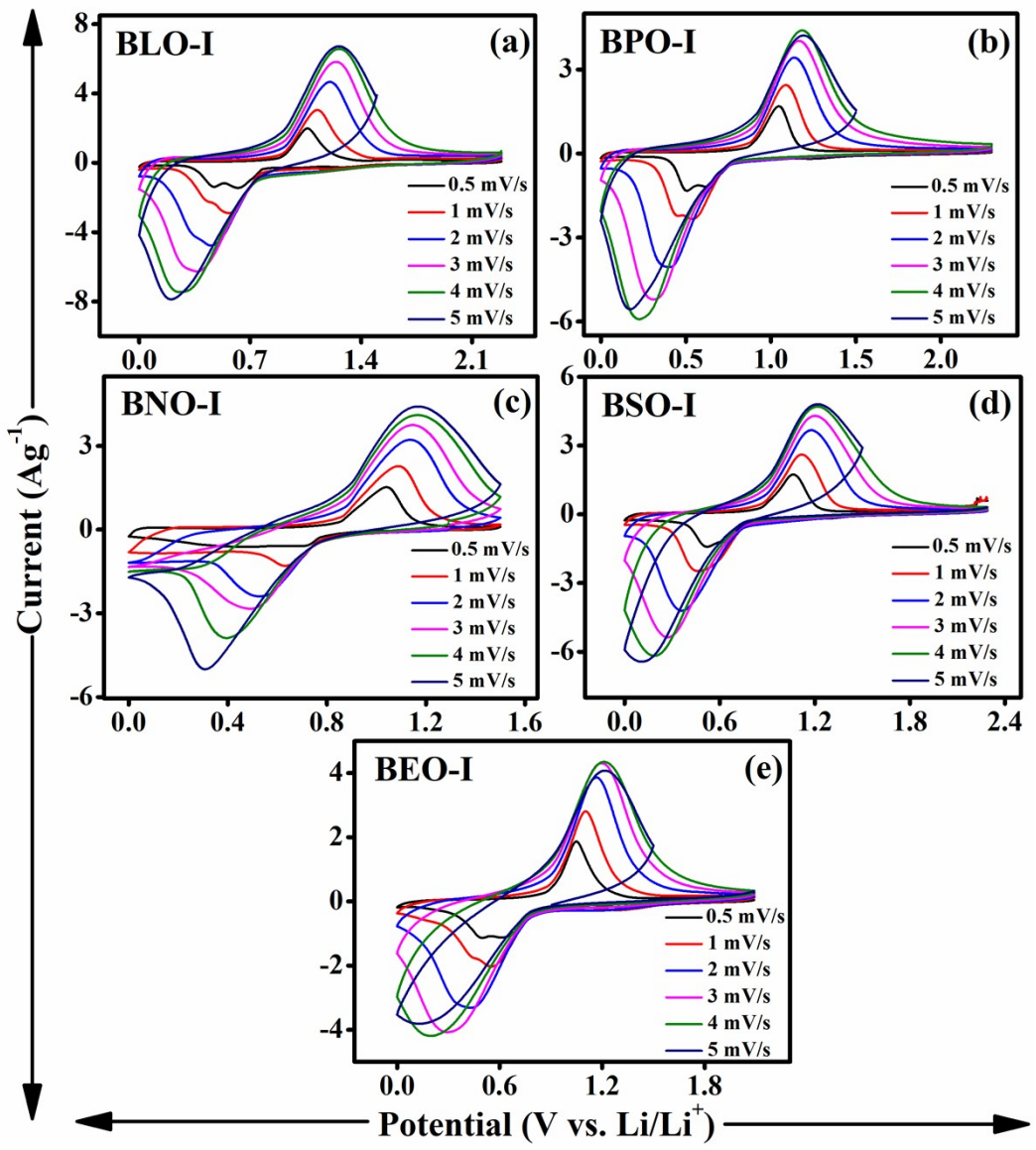

Fig. S13 Cyclic voltammograms with different scan rates of (a) BLO-I, (b) BPO-I, (c) BNO-I, (d) BSO-I, and (e) BEO-I.

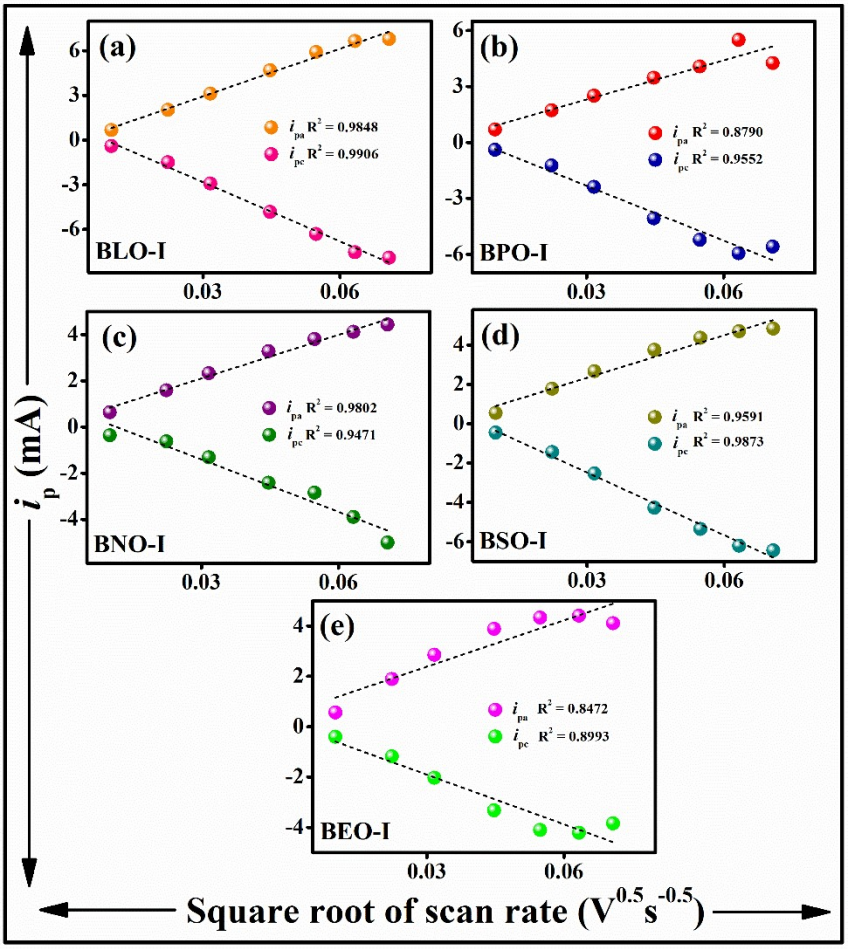

Fig. S14 Relationship between anodic and cathodic peak current (i_{pa} and i_{pc}) and the square root of scanning rates ($\upsilon^{1/2}$) of BLO-I, BPO-I, BNO-I, BSO-I, and BEO-I samples.

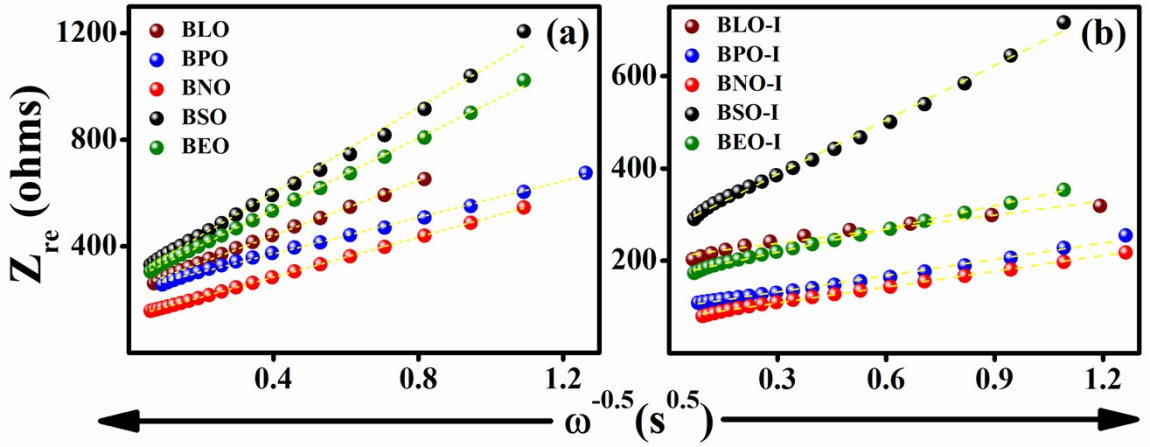

Fig. S15 Frequency response of real part of the impedance of (a) BLO, BPO, BNO, BSO, and BEO samples, (b) BLO-I, BPO-I, BNO-I, BSO-I, and BEO-I samples.

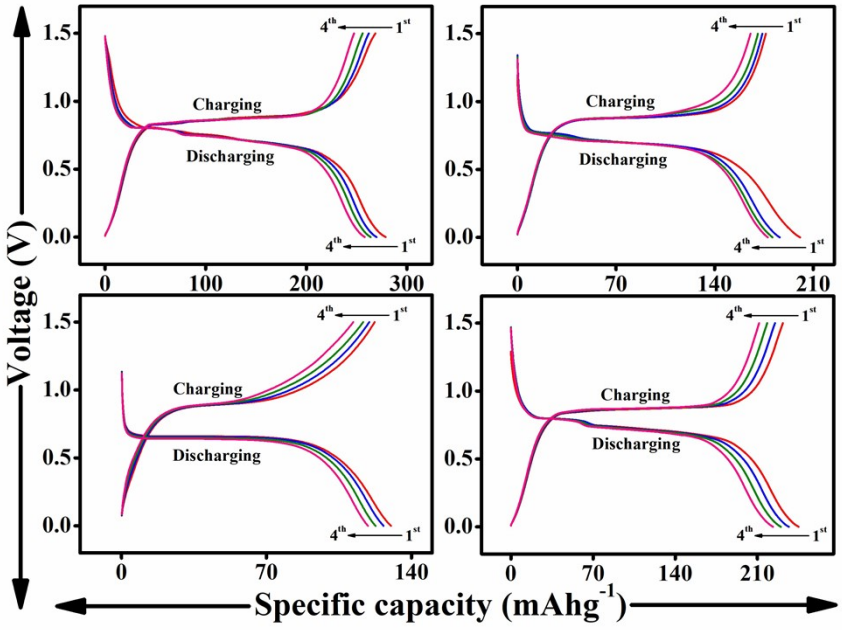

Fig. S16 Galvanostatic charge-discharge performance of iodine intercalated $Bi_{0.775}La_{0.225}O_{1.5}$ sample at (a) 10, (b) 20, (c) 50, (d) repeat 10 mAg^{-1}.

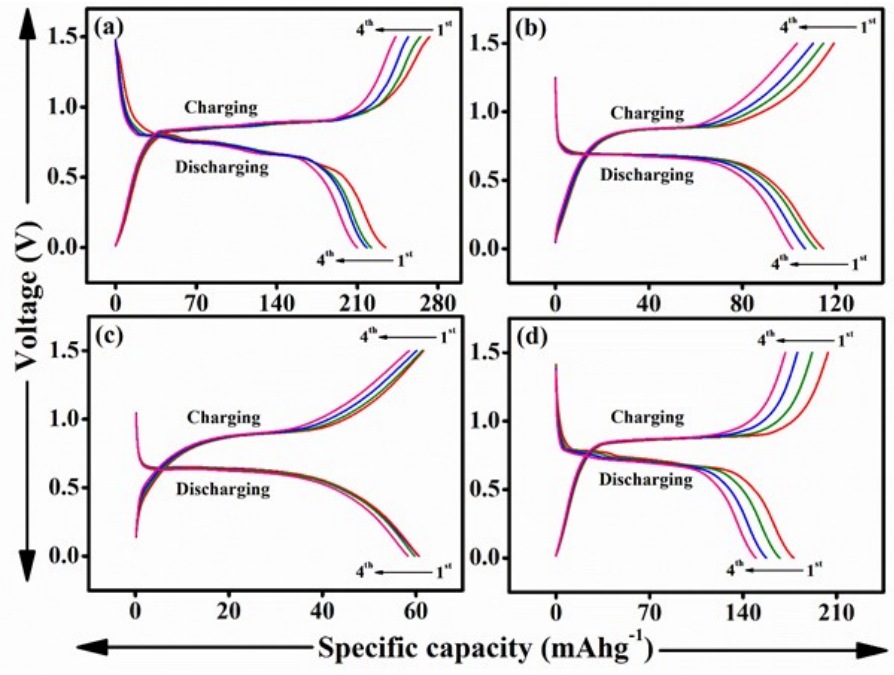

Fig. S17 Galvanostatic charge-discharge performance of iodine intercalated $Bi_{0.775}Pr_{0.225}O_{1.5}$ sample at (a) 10, (b) 20, (c) 50, (d) repeat 10 mAg^{-1}.

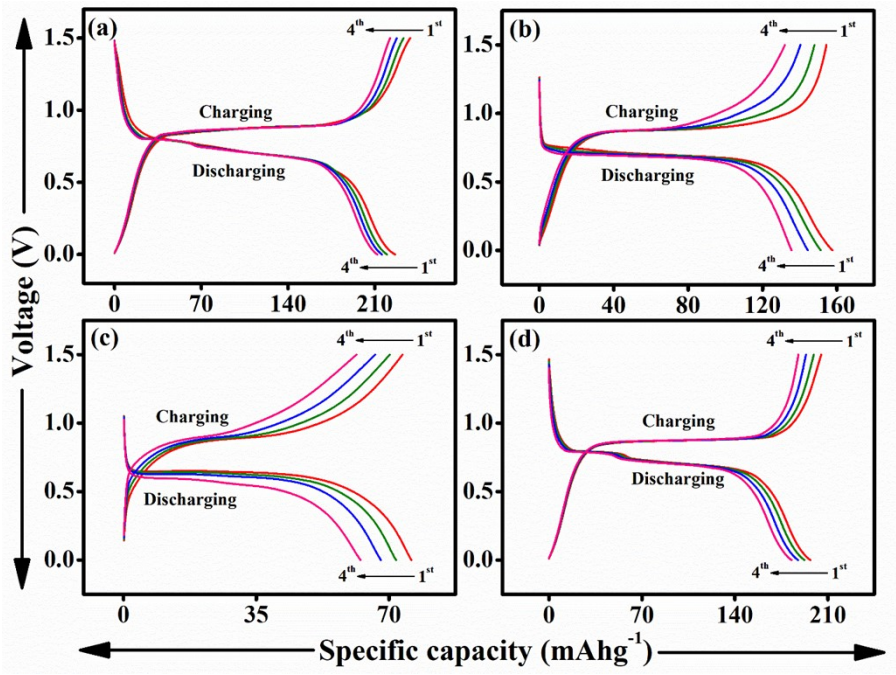

Fig. S18 Galvanostatic charge-discharge performance of iodine intercalated $Bi_{0.775}Nd_{0.225}O_{1.5}$ sample at (a) 10, (b) 20, (c) 50, and (d) repeat 10 mAg^{-1}.

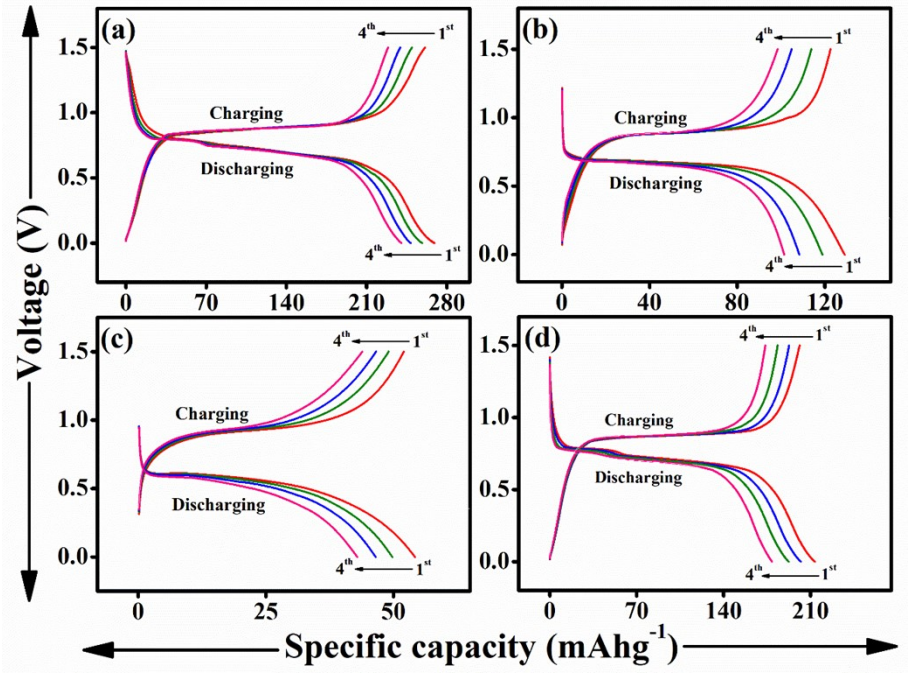

Fig. S19 Galvanostatic charge-discharge performance of iodine intercalated $Bi_{0.775}Sm_{0.225}O_{1.5}$ sample at (a) 10, (b) 20, (c) 50, (d) repeat 10 mAg^{-1}.

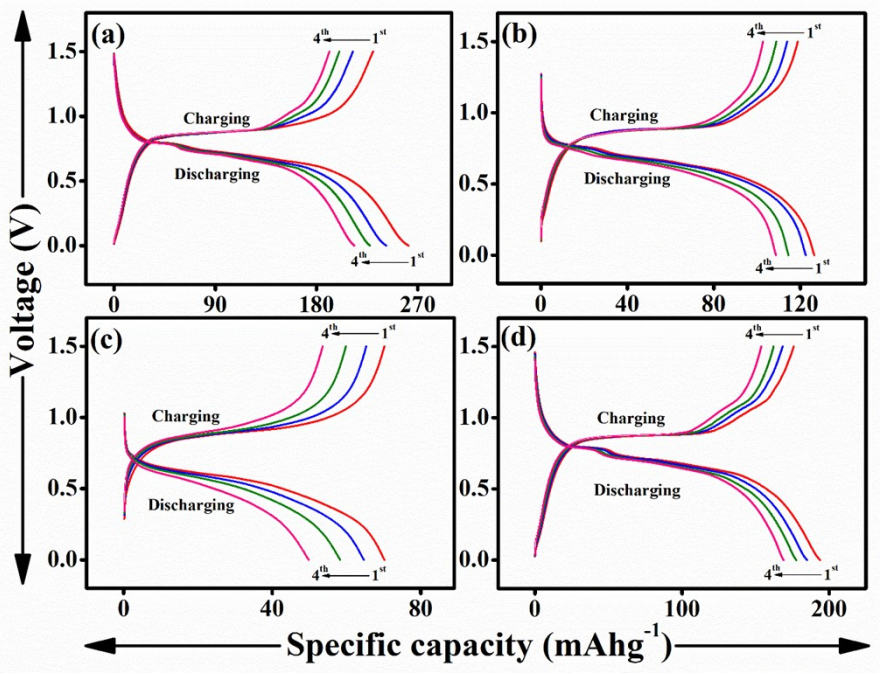

Fig. S20 Galvanostatic charge-discharge performance of iodine intercalated $Bi_{0.775}Eu_{0.225}O_{1.5}$ sample at (a) 10, (b) 20, (c) 50, (d) repeat 10 mAg^{-1}.

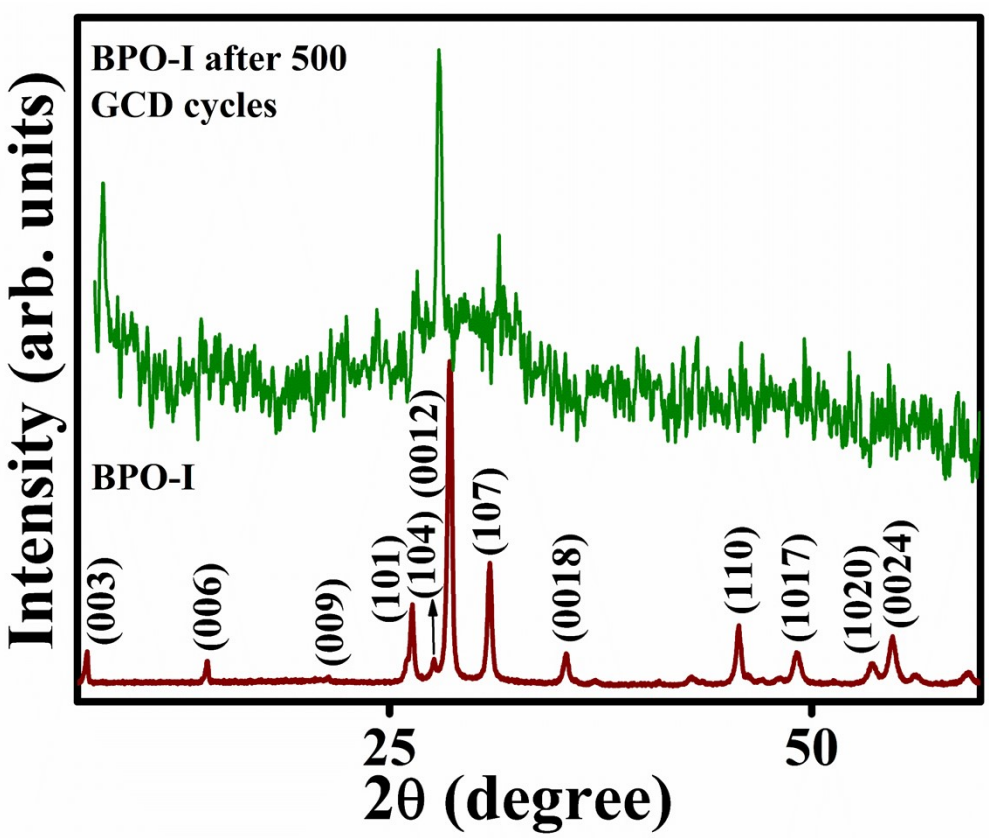

Fig. S21 PXRD pattern of the electroactive BPO-I before and after its use in charge-discharge experiments (500 cycles)

Table S1 Lattice parameters estimated from the lattice refinement of the PXRD patterns of the $Bi_{0.775}Ln_{0.225}O_{1.5}$ (Ln = La, Pr, Nd, Sm, and Eu) samples by the Le Bail method in hexagonal symmetry (*R*-3*m* (#166)).

Formula	**$Bi_{0.775}La_{0.225}O_{1.5}$**	**$Bi_{0.775}Pr_{0.225}O_{1.5}$**	**$Bi_{0.775}Nd_{0.225}O_{1.5}$**	**$Bi_{0.775}Sm_{0.225}O_{1.5}$**	**$Bi_{0.775}Eu_{0.225}O_{1.5}$**
a (Å)	4.0235 (4)	4.0081 (5)	3.9814 (7)	3.9879 (7)	3.9593 (9)
c (Å)	27.7345 (5)	27.6138 (5)	27.4886 (8)	27.5040 (5)	27.3165 (2)
Cell volume ($Å^3$)	388.834 (8)	384.195 (8)	378.201 (8)	376.816 (7)	370.849 (2)
Temp. (°C)	25	25	25	25	25
No. of data points	8499	8499	8499	3235	3235
2θ range	15-100°	15-100°	15-100°	15-100°	15-100°
R_p	0.0607	0.0780	0.1304	0.0530	0.0593
R_{wp}	0.0806	0.1015	0.1766	0.0685	0.0750
χ^2	0.7033	0.8993	0.8914	1.500	1.835

Table S2 Lattice parameters estimated from the lattice refinement of the PXRD patterns of the iodine intercalated $Bi_{0.775}Ln_{0.225}O_{1.5}$ (Ln = La, Pr, Nd, Sm, and Eu) samples by the Le Bail method in hexagonal symmetry (*R*-3*m* (#166)).

Formula	**$Bi_{0.775}La_{0.225}O_{1.5}$**	**$Bi_{0.775}Pr_{0.225}O_{1.5}$**	**$Bi_{0.775}Nd_{0.225}O_{1.5}$**	**$Bi_{0.775}Sm_{0.225}O_{1.5}$**	**$Bi_{0.775}Eu_{0.225}O_{1.5}$**
a (Å)	3.9768 (8)	3.9704 (7)	3.9496 (8)	3.9487 (7)	3.9098 (22)
c (Å)	37.465 (24)	37.456 (14)	37.3654 (14)	37.3125 (15)	36.753 (5)
Cell volume ($Å^3$)	513.133 (27)	511.366 (14)	504.785 (15)	503.844 (15)	486.57 (5)
Temp. (°C)	25	25	25	25	25
No. of data points	9701	9700	9701	9701	3237
2θ range	5-90°	5-90°	5-90°	5-90°	5-90°
R_p	0.0565	0.0579	0.0566	0.0624	0.0611
R_{wp}	0.0739	0.0761	0.0745	0.0822	0.0775
χ^2	0.8026	0.8847	0.7884	0.6813	2.01

Table S3 Comparison of electrochemical performance of 2D materials as anode in LIBs.

2D Materials based on	**System**	**Initial discharge capacity (mAh/g)/ current density(mA/g)**	**Ref.**
Chalcogenides	GaS nanosheets GaSe nanosheets	1730/100 1100/300	1
	WS_2 NTs	768/100	2
	CoSe	550/100	3
	$MoSe_2$	851.1/100	4
	TiS_2 Nanosheets	~300/50	5
	NiS $NiSe_2$	1311/100 992/100	6
	GeS GeS_2 SnS SnS_2	1232/0.1C 1099/0.1C 867/0.1C 647/0.1C	7
MXene	V_2C	467/50	8
	Ti_2C	160/0.1C	9
	Nb_2CT_x	985/50	10
	Ti_3C_2T	123.6/1C	11
	Mo_2C	136/10	12
	Few-layer Nb_2CT_x	746/50	13
Bismuth oxyhalides	$Bi_{0.7}Fe_{0.3}OCl$ nanosheets	555/50	14
	BiOCl BiOBr	633/100 605/100	15
	BiOI	717/30	16
Iodine intercalated $Bi_{0.775}La_{0.225}O_{1.5}$		**278/10**	**This work**
Iodine intercalated $Bi_{0.775}Pr_{0.225}O_{1.5}$		**234/10**	
Iodine intercalated $Bi_{0.775}Nd_{0.225}O_{1.5}$		**227/10**	
Iodine intercalated $Bi_{0.775}Sm_{0.225}O_{1.5}$		**250/10**	
Iodine intercalated $Bi_{0.775}Eu_{0.225}O_{1.5}$		**273/10**	

References

1 C. Zhang, S. H. Park, O. Ronan, A. Harvey, A. Seral-Ascaso, Z. Lin, N. McEvoy, C. S. Boland, N. C. Berner, G. S. Duesberg, and P. Rozier, *Small* 2017, **13**, 1701677-1701688.

2 R. Chen, T. Zhao, W. Wu, F. Wu, L. Li, J. Qian, R. Xu, H. Wu, H. M. Albishri, A. S. Al-Bogami, and D. A. El-Hady, *Nano Lett.* 2014, **14**, 5899-5904.

3 Y. Li, Y. Xu, Z. Wang, Y. Bai, K. Zhang, R. Dong, Y. Gao, Q. Ni, F. Wu, Y. Liu, and C. Wu, *Adv. Energy Mater.* 2018, **8**, 1800927-1800935.

4 Y. Liu, M. Zhu, and D. Chen, *J. Mater. Chem. A*, 2015, **3**, 11857-11862.

5 D. Y. Oh, Y. E. Choi, D. H. Kim, Y. G. Lee, B. S. Kim, J. Park, H. Sohn, and Y. S. Jung, *J. Mater. Chem. A* 2016, **4**, 10329-10335.

6 H. Fan, H. Yu, X. Wu, Y. Zhang, Z. Luo, H. Wang, Y. Guo, S. Madhavi, and Q. Yan, *ACS Appl. Mater. Interfaces* 2016, **8**, 25261-25267.

7 H. S. Im, Y. R. Lim, Y. J. Cho, J. Park, E. H. Cha, and H. S. Kang, *J. Phys. Chem. C* 2014, **118**, 21884-21888.

8 F. Liu, J. Zhou, S. Wang, B. Wang, C. Shen, L. Wang, Q. Hu, Q. Huang, and A. Zhou, *J. Electrochem. Soc.* 2017, **164**, A709-A713.

9 M. Naguib, J. Come, B. Dyatkin, V. Presser, P. L. Taberna, P. Simon, M. W. Barsoum, and Y. Gogotsi, *Electrochem. Commun.* 2012, **16**, 61-64.

10 J. Zhao, J. Wen, J. Xiao, X. Ma, J. Gao, L. Bai, H. Gao, X. Zhang, and Z. Zhang, *J. Energy Chem.* 2021, **53**, 387-395.

11 D. D. Sun, M. S. Wang, Z. Y. Li, G. X. Fan, L. Z. Fan, and A. G. Zhou, *Electrochem. Commun.* 2014, **47**, 80-83.

12 J. Mei, G. A. Ayoko, C. Hu, J. M. Bell, and Z. Sun, *Sustain. Mater. Technol.* 2020, **25**, e00156.

13 J. B. Zhao, J. Wen, L. N. Bai, J. P. Xiao, R. D. Zheng, X. Y. Shan, L. Li, H. Gao, and X. T. Zhang, *Dalton Trans.* 2019, **48**, 14433-14439.

14 Y. Myung, J. Choi, F. Wu, S. Banerjee, E. H. Majzoub, J. Jin, S. U. Son, P. V. Braun, and P. Banerjee, *ACS Appl. Mater. Interfaces* 2017, **9**, 14187-14196.

15 L. Ye, L. Wang, H. Xie, Y. Su, X. Jin, and C. Zhang, *Energy Technol.* 2015, **3**, 1115-1120.

16 C. Chen, P. Hu, X. Hu, Y. Mei, and Y. Huang, *Chem. Commun.* 2015, **51**, 2798-2801.